primers with which to assay *RPS4X* methylation in particular species; primer and underlying sequences have been deposited at GenBank: human, accession no. G36429; chimp and gorilla, G36430 and G36431; rabbit, G36432; guinea pig, G36433; mouse, G36434; rat, G36435; lemming, G36436; squirrel, G36437; dog, G36438; anteater, G36439; hedgehog, G36440; whale, G36441; and horse, G36442. For *SMCX*, PCR primers were chosen from CpG-island sequences found to be conserved between human and mouse: CCTCGGGCCCACCATG-GAG and CTGATTTTCGCGATGTAGCC amplify a 117-bp product that includes three CCGG sites in humans and two in mice. We selected these conserved *SMCX* primers after sequencing 5′ portions of the mouse transcript (GenBank AF0398940; obtained by 5′ RACE cloning) and comparing these with previously published 5′ human *SMCX* sequences[20].

Y-chromosome homologues. We searched for Y-specific homologues of *ZFX/ZFY* and *SMCX/SMCY* in mammalian species by Southern blotting of *Eco*RI-digested male and female genomic DNAs. For *ZFY*, we used two hybridization probes in separate experiments, with entirely concordant results (Figs 2 and 3): (1) a 395-bp genomic *Bss*HII fragment[10] from the 5′ CpG island of human *ZFY*, and (2) pDP1007, a 1.3-kb genomic fragment containing the zinc-finger exon[26] of human *ZFY*. Probes were labelled with ^{32}P by random-primer synthesis and hybridized overnight to Southern blots at 67 °C (65 °C for pDP1007) in 1 mM EDTA, 0.5 M $NaPO_4$ pH 7.2 and 7% sodium dodecyl sulphate (SDS). Blots were then washed three times for 20 min each at 62 °C in 0.1 × SSC (1 × SSC = 0.15 M NaCl, 15 mM Na citrate pH 7.4), 0.1% SDS and exposed at −80 °C with X-ray film backed with an intensifying screen for one day. The *SMCY* hybridization probe (pCM4) and conditions were described previously[20].

We also searched for Y-chromosome homologues of *RPS4X/RPS4Y* and *SMCX/SMCY* in particular species by cDNA selection, or by screening cDNA libraries. In cDNA selection[27], human *RPS4Y* coding sequence (as selector) was hybridized at 55 °C to cDNA libraries (Clontech) prepared from adult male rat, rabbit, dog or cattle liver. Selection products were cloned into plasmid vectors and sequenced. cDNA libraries prepared from adult male dog liver (Clontech) and adult male opossum spleen (Stratagene) were screened with the entire human *RPS4Y* coding sequence as probe, at low stringency (overnight hybridization at 58 °C in 1 mM EDTA, 0.5 M $NaPO_4$ pH 7.2, 7% SDS; subsequent washing three times for 20 min each at 50 °C in 1 × SSC, 0.1% SDS). Once dog and opossum *RPS4X* clones were identified, by sequencing, these were used as probes for high-stringency rescreening of their respective libraries (hybridization at 65 °C and washes at 65°C in 0.1 × SSC, 0.1% SDS). We anticipated that *RPS4Y* clones, if present, would be detected in the low-stringency screen but not in the high-stringency screen. In this manner, we identified opossum *RPS4Y* (and *RPS4X*) cDNA clones, confirmed by sequencing (GenBank AF051137 and AF051136, respectively) and mapping studies (K.J. and D.C.P., unpublished results; complete description will be published elsewhere), but in dog we detected only *RPS4X* clones. Similarly, we screened a cDNA library (Clontech) prepared from adult male rabbit liver at low stringency using a 370-bp mouse *Smcx* cDNA fragment (prepared from clone pCM4 (ref. 20) by PCR using primers CCTTCCAAGTTCAACAGTT ATGG and CATACGTATGACTCAATAAACTGGG), identifying 13 *SMCX* but no *SMCY* clones.

Received 25 March; accepted 9 June 1998.

1. Ohno, S. *Sex Chromosomes and Sex-linked Genes* (Springer, Berlin, 1967).
2. Graves, J. A. & Schmidt, M. M. Mammalian sex chromosomes: design or accident? *Curr. Opin. Genet. Dev.* **2,** 890–901 (1992).
3. Lyon, M. F. Evolution of X-chromosome inactivation in mammals. *Nature* **250,** 651–653 (1974).
4. Disteche, C. M. The great escape. *Am. J. Hum. Genet.* **60,** 1312–1315 (1997).
5. Cross, S. H. & Bird, A. P. CpG islands and genes. *Curr. Opin. Genet. Dev.* **5,** 309–314 (1995).
6. Tribioli, C. *et al.* Methylation and sequence analysis around *Eag*I sites: identification of 28 new CpG islands in Xq24-Xq28. *Nucl. Acids Res.* **20,** 727–733 (1992).
7. Migeon, B. R. *et al.* Adrenoleukodystrophy: evidence for X linkage, inactivation, and selection favoring the mutant allele in heterozygous cells. *Proc. Natl Acad. Sci. USA* **78,** 5066–5070 (1981).
8. Brown, C. J., Carrel, L. & Willard, H. F. Expression of genes from the human active and inactive X chromosomes. *Am. J. Hum. Genet.* **60,** 1333–1343 (1997).
9. Schneider-Gädicke, A., Beer-Romero, P., Brown, L. G., Nussbaum, R. & Page, D. C. *ZFX* has a gene structure similar to *ZFY*, the putative human sex determinant, and escapes X inactivation. *Cell* **57,** 1247–1258 (1989).
10. Luoh, S. W. *et al.* CpG islands in human *ZFX* and *ZFY* and mouse *Zfx* genes: sequence similarities and methylation differences. *Genomics* **29,** 353–363 (1995).
11. Ashworth, A., Rastan, S., Lovell-Badge, R. & Kay, G. X-chromosome inactivation may explain the difference in viability of XO humans and mice. *Nature* **351,** 406–408 (1991).
12. Adler, D. A., Bressler, S. L., Chapman, V. M., Page, D. C. & Disteche, C. M. Inactivation of the *Zfx* gene on the mouse X chromosome. *Proc. Natl Acad. Sci. USA* **88,** 4592–4595 (1991).
13. Fisher, E. M. *et al.* Homologous ribosomal protein genes on the human X and Y chromosomes: escape from X inactivation and possible implications for Turner syndrome. *Cell* **63,** 1205–1218 (1990).
14. Zinn, A. R. *et al.* Inactivation of the *Rps4* gene on the mouse X chromosome. *Genomics* **11,** 1097–1101 (1991).
15. Aguinik, A. I. *et al.* A novel X gene with a widely transcribed Y-linked homologue escapes X-inactivation in mouse and human. *Hum. Mol. Genet.* **3,** 879–884 (1994).
16. Wu, J. *et al.* Isolation and characterization of *XE169*, a novel human gene that escapes X-inactivation. *Hum. Mol. Genet.* **3,** 153–160 (1994).
17. Wu, J. *et al.* The murine *Xe169* gene escapes X-inactivation like its human homologue. *Nature Genet.* **7,** 491–496 (1994).
18. Charlesworth, B. The evolution of chromosomal sex determination and dosage compensation. *Curr. Biol.* **6,** 149–162 (1996).
19. Rice, W. R. Evolution of the Y sex chromosome in animals. *BioScience* **46,** 331–343 (1996).
20. Aguinik, A. I., Mitchell, M. J., Lerner, J. L., Woods, D. R. & Bishop, C. E. A mouse Y chromosome gene encoded by a region essential for spermatogenesis and expression of male-specific minor histocompatibility antigens. *Hum. Mol. Genet.* **3,** 873–878 (1994).
21. Mahaffey, C. L. *et al.* Intron/exon structure confirms that mouse *Zfy1* and *Zfy2* are members of the *ZFY* gene family. *Genomics* **41,** 123–127 (1997).
22. Omoe, K. & Endo, A. Relationship between the monosomy X phenotype and Y-linked ribosomal protein S4 (*Rps4*) in several species of mammals: a molecular evolutionary analysis of *Rps4* homologs. *Genomics* **31,** 44–50 (1996).
23. Muller, H. J. Evidence of the precision of genetic adaptation. *Harvey Lect.* **43,** 165–229 (1950).
24. Adler, D. A. *et al.* Evidence of evolutionary up-regulation of the single active X chromosome in mammals based on *Clc4* expression levels in Mus spretus and Mus musculus. *Proc. Natl Acad. Sci. USA* **94,** 9244–9248 (1997).
25. Goldman, M. A. The chromatin domain as a unit of gene regulation. *BioEssays* **9,** 50–55 (1988).
26. Page, D. C. *et al.* The sex-determining region of the human Y chromosome encodes a finger protein. *Cell* **51,** 1091–1104 (1987).
27. Lovett, M., Kere, J. & Hinton, L. M. Direct selection: a method for the isolation of cDNAs encoded by large genomic regions. *Proc. Natl Acad. Sci. USA* **88,** 9628–9632 (1991).
28. Novacek, M. J. Mammalian phylogeny: shaking the tree. *Nature* **356,** 121–125 (1992).
29. Sinclair, A. H. *et al.* Sequences homologous to *ZFY*, a candidate human sex-determining gene, are autosomal in marsupials. *Nature* **336,** 780–783 (1988).
30. D'Esposito, M. *et al.* A synaptobrevin-like gene in the Xq28 pseudoautosomal region undergoes X inactivation. *Nature Genet.* **13,** 227–229 (1996).

Acknowledgements. We thank the New England Aquarium, the San Diego Zoo, the Duke Primate Center, K. Fredga and K. Campbell for help in obtaining animal specimens; A. Agulnik for a mouse *Smcx* cDNA clone; D. Graur and B. Lahn for helpful discussions; J. Graves for permission to cite unpublished work; J. Cook-Chrysos for graphic art; and D. Bartel, B. Charlesworth, A. Chess, C. Disteche, G. Fink, J. Graves, R. Jaenisch, T. Kawaguchi, M. L. Pardue, D. Schlessinger, C. Sun, H. Willard and A. Zinn for comments on the manuscript. This work was supported by the National Institutes of Health and the Howard Hughes Medical Institute.

Correspondence and requests for materials should be addressed to D.C.P. (e-mail: dcpage@wi.mit.edu).

Signal-dependent noise determines motor planning

Christopher M. Harris* & Daniel M. Wolpert†

** Department of Ophthalmology and Visual Sciences Unit, Great Ormond Street Hospital for Children NHS Trust, and Institute of Child Health, University College London, London WC1N 3JH, UK*

† Sobell Department of Neurophysiology, Institute of Neurology, Queen Square, University College London, London WC1N 3BG, UK

When we make saccadic eye movements or goal-directed arm movements, there is an infinite number of possible trajectories that the eye or arm could take to reach the target[1,2]. However, humans show highly stereotyped trajectories in which velocity profiles of both the eye and hand are smooth and symmetric for brief movements[3,4]. Here we present a unifying theory of eye and arm movements based on the single physiological assumption that the neural control signals are corrupted by noise whose variance increases with the size of the control signal. We propose that in the presence of such signal-dependent noise, the shape of a trajectory is selected to minimize the variance of the final eye or arm position. This minimum-variance theory accurately predicts the trajectories of both saccades and arm movements and the speed–accuracy trade-off described by Fitt's law[5]. These profiles are robust to changes in the dynamics of the eye or arm, as found empirically[6,7]. Moreover, the relation between path curvature and hand velocity during drawing movements reproduces the empirical 'two-thirds power law'[8,9]. This theory provides a simple and powerful unifying perspective for both eye and arm movement control.

The trajectories of eye and arm movements (that is, the change in position and velocity over time) are not inevitable consequences of

the mechanical properties of muscles, but reflect an orchestrated pattern of neural activation by motor and pre-motor neurons. For saccadic eye movements, it has been proposed that trajectories are selected to minimize the time to reach the target[10]. For a linear system, the minimum-time requirement results in 'bang-bang' control, where the control signal is instantaneously switched between its maximum positive and negative values to accelerate and decelerate the eye. However, it is difficult to generate the observed symmetrical saccadic velocity profiles with bang-bang control signals[11,12]. For arm movements, it has been suggested that trajectories are selected to optimize a cost that is integrated over the movement, such as jerk (rate of change of acceleration)[13,14] or torque change[15]. However, there has been no principled explanation why the central nervous system should have evolved to optimize such quantities, other than that these models predict smooth trajectories. Indeed, the advantage of smoothness of movement still remains unexplained. Furthermore, how the central nervous system could estimate complex quantities, such as jerk or torque change, and then integrate them over the duration of a trajectory is also unknown.

We propose that minimizing the variance of the eye or arm's position, in the presence of biological noise, is the underlying determinant of trajectory planning. Noise in the final neural control signal (that is, noise in the firing of motor neurons) will cause trajectories to deviate from the desired path. These deviations will be accumulated over the duration of a movement, leading to variability in the final position. If the noise were independent of the control signal[16], then the accumulated error would be minimized by making the movement as rapidly as possible, as in bang-bang control for linear systems. However, here we assume that the noise in the neural control signal increases with the mean level of the signal. This is based on the empirical observation that the standard deviation of motor-neuronal firing increases with the mean level, with a coefficient of variation between 10 and 25% (refs 17, 18). This assumption of signal-dependent noise is also consistent with psychophysical observations that the variability of motor errors increases with the magnitude of the movement, as captured by the empirical Fitt's law[5]. In the presence of such signal-dependent noise, moving as rapidly as possible requires large control signals, which would increase the variability in the final position. As the resulting inaccuracy of the movement may lead to task failure or require further corrective movements, moving very fast becomes counterproductive[19,20]. Accuracy could be improved by having low control signals, but the movement will be slow. Thus, signal-dependent noise inherently imposes a trade-off between movement

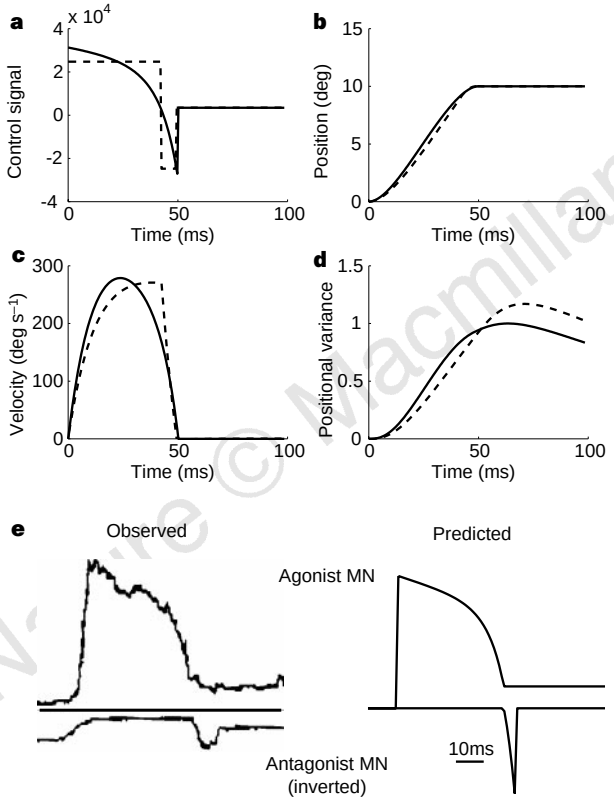

Figure 1 A comparison of bang-bang (dashed line) and minimum-variance (solid line) control for a 10 degree saccade with a duration of 50 ms. **a**, Neural control signals; **b**, average position profiles of trajectories across repeated movements are similar; **c**, velocity profiles show a marked difference in their degree of symmetry; **d**, positional variance (obtained from equation (1) in Methods) which represents the spread of the eye position across repeated trials, about the mean position shown in **b**. Note that the variance continues to evolve after the mean position has become steady. The eye was modelled as a second-order linear system with time constants of 224 and 13 ms. The variances have been scaled so that the peak for the minimum-variance model is unity. **e**, Empirical (from ref. 22, with permission) and predicted motor neuronal firing of agonist and antagonist eye muscles in monkey for a 12 degree saccade. To model the monkey's faster plant, time constants of 150 and 7 ms were used for this simulation. The predicted motoneuronal activity was derived from the control signal by splitting it into positive (agonist) and negative (antagonist) parts (the final tonic level of the antagonist has not been modelled). Note that temporal jitter of firing is likely to broaden and lower the predicted sharp antagonist peak.

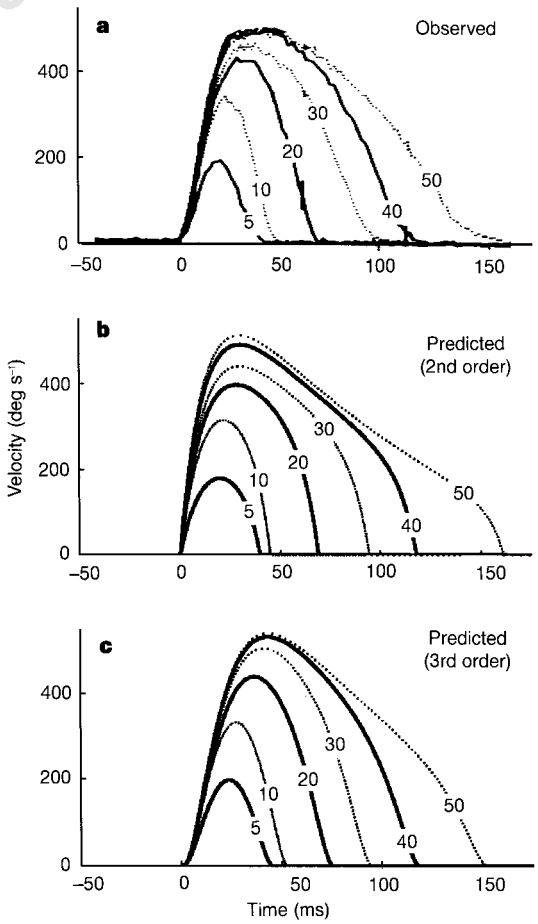

Figure 2 Comparison of empirical and predicted saccade trajectories. **a**, Velocity profiles of actual horizontal saccadic eye movements ranging in amplitude from 5 to 50 degrees (taken from ref. 4, with permission). Saccades below 30 degrees are symmetric, whereas larger saccades are asymmetric with a longer decelerative phase. **b**, Theoretical optimal trajectories for minimizing positional variance with signal-dependent noise for a second-order linear model of the eye with time constants of 224 and 13 ms. **c**, Theoretical optimal trajectories for a third-order linear model of the eye with the additional time constant of 10 ms. The predicted trajectories show the change in symmetry with saccade amplitude.

duration and terminal accuracy. The key point is that for a given amplitude and duration of movement, the final positional variance will depend critically on the actual neural commands and the subsequent velocity profile. We propose that the temporal profile of the neural command is selected so as to minimize the final positional variance for a specified movement duration, or equivalently to minimize the movement duration for a specified final positional variance determined by the task.

We assume that neural commands have signal-dependent noise whose standard deviation increases linearly with the absolute value of the neural control signal. On the basis of this single assumption, we determined the optimal trajectories of the eye and arm that minimized the total positional variance during the immediate post-movement period (see Methods). For saccades, we considered a commonly used second-order linear system[21], in which the minimum-variance and bang-bang solutions were compared for a 50-ms 10-degree movement (Fig. 1). Both the control strategies reach the target position in the same time (Fig. 1b), but the positional variance in the post-movement period is significantly lower for the minimum-variance solution (Fig. 1d). Although on average the eye is on target, with zero velocity at the end of the movement (Fig. 1b), on any single trajectory there will be a positional error and a non-zero velocity at the end of the movement due to the effect of the signal-dependent noise. Therefore, as seen in Fig. 1d, the positional variance can continue to change after the movement. Thus to minimize deviations from the final position, it is necessary to minimize variance over a post-movement period. The minimum-variance solution results in a smooth symmetric velocity profile, in contrast to the asymmetric profile produced by bang-bang control (Fig. 1c). The model is also in qualitative agreement with observed agonist and antagonist motoneuronal firing patterns[22] (Fig. 1e).

Over a range of amplitudes, the minimum-variance solutions (Fig. 2b) also capture the important features of natural saccadic movements (Fig. 2a)—symmetric short movements and asymmetric long movements with an extended deceleration phase[4]. With a third-order model of the eye, the optimal trajectories capture the bell-shaped trajectories observed empirically (Fig. 2c). The optimal trajectories also show a similar rise time for all saccades and a saturation in the peak velocity for saccade amplitudes above ~30 degrees, as is observed experimentally. Although it has been proposed that this saturation arises from limits on the control signal[10], the minimum-variance model predicts this saturation without any such limits. The shapes of trajectories for amplitudes under 20 degrees were insensitive to modest changes in the time constants of the system, whereas these parameters had a much bigger effect on the slower movements. This is consistent with the general observation that the speed and duration of large saccades have greater variability within and between individuals than those of small saccades. For brief movements, the order of the plant is the major determinant of the optimal trajectory. In the limit, for infinitely brief movements, the highest-order term dominates and the model predicts symmetrical trajectories[12]. In Fig. 2, trajectories for second- and third-order models are shown; the trajectories for models of higher order are very similar to the third-order model. For longer movements, the lower-order terms become more important, leading to asymmetrical and complex optimal trajectories.

For arm movements, we first considered a simple one-dimensional fourth-order linear model which captures the muscle dynamics and the arm's skeletal inertia and viscosity[23] (see Methods). The optimal trajectory for a fast movement (Fig. 3b), in which feedback was assumed to play a negligible role, shows the typical bell-shaped velocity profile seen in natural movements[24] (Fig. 3a). The profile is again insensitive to changes in the plant, so that even when the inertia and viscosity of the arm or the time constants of the muscle are individually halved or doubled, the optimal profile remains essentially unchanged (Fig. 3c). This is consistent with the observation that when the arm is subject to elastic, viscous or inertial loads, the bell-shaped velocity profile is regained after a period of adaptation[6,7,25–28].

For arm movements, the required accuracy varies with the task, as for example in the difference between pointing to someone in a room compared with threading a needle. When pointing at targets, it is empirically observed that movement duration increases with the accuracy demanded by the task. This relationship is captured empirically by Fitt's law, in which the required accuracy is determined by the width of the target (Fig. 4a). For any given movement duration, signal-dependent noise places a lower limit on the final positional variance given by the minimum-variance trajectory. Conversely, given a movement accuracy constraint, specified in terms of final positional variance, there is a minimum duration of movement which can achieve this. We propose that this minimum duration trajectory will be chosen, given the limits of the final endpoint variance imposed by the task. By assuming a linear relationship between the required final endpoint standard deviation

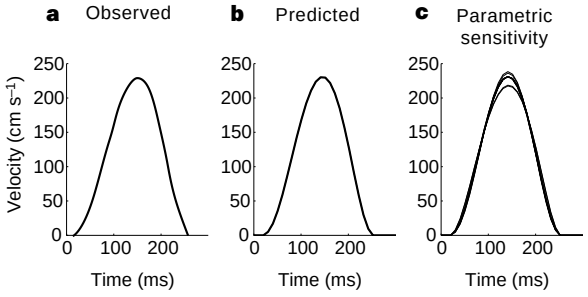

Figure 3 Comparison of empirical and theoretical arm velocity profiles. **a**, Velocity profile of the hand in a typical fast arm movement (taken from ref. 24, with permission). **b**, Theoretical optimal trajectory for minimizing post-movement variance with signal-dependent noise for a second-order skeletal model of a one-dimensional arm with inertia 0.25 kg m^2 and viscosity 0.2 N ms rad^{-1} driven by a second-order linear muscle with time constants of 30 and 40 ms (parameters taken from ref. 23). **c**, Eight velocity profiles for the model in **b** in which the inertia, viscosity and time constants are individually doubled or halved. The trajectory is essentially invariant to these large changes in the dynamics of the arm.

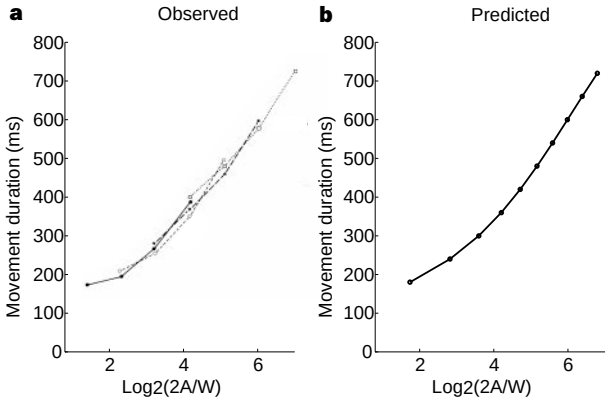

Figure 4 Comparison of empirical and predicted arm movement durations. **a**, Fitt's law relates movement duration (T) to the movement amplitude (A) and target width (W shown as different symbols and lines) according to $T = a + b \log_2(2A/W)$, where a and b are constants. Empirical data from ref. 30 (with permission). This shows the typical increase in movement duration as either the amplitude of movement increases or the target width decreases. **b**, Predicted movement durations for the minimum-variance model in the presence of signal-dependent noise. The movement duration was calculated as the shortest possible, given that the target width places an upper limit on the endpoint positional standard deviation (see Methods). Note the predictions for different widths, W, completely overlap.

and the target width, Fitt's law emerges as a consequence of signal-dependent noise (Fig. 4b).

We next considered a two-joint nonlinear model of the arm moving in the horizontal plane (see Methods). The optimal trajectories for point-to-point movements again showed bell-shaped velocity profiles (Fig. 5d) with gently curved hand paths (Fig. 5b), as observed empirically (Fig. 5a, c)[15]. For drawing movements, it has been found that hand velocity (V) decreases as the radius of curvature of the path (R) decreases—this has been formulated as the 'two-thirds power law', $V = KR^{(1-\beta)}$, where K is a constant and $\beta \approx 2/3$ (refs 8, 9). We derived the trajectory that would minimize the positional variance of the hand when repetitively drawing ellipses (see Methods). The optimal trajectory shows the typical slowing down as the curvature increases (Fig. 5e) and reproduces the two-thirds power law, as seen by the regression line in Fig. 5f (slope of 0.32, giving $\beta = 0.68$). This shows that the minimum-variance trajectory predicts the two-thirds power law.

From these analyses, we see that the trajectories of both saccadic eye movements and arm movements can be described as trajectories that minimize post-movement variance in the presence of signal-dependent noise on the control signal. This approach has several important ramifications. Primarily, it provides a biologically plausible theoretical underpinning for both eye and arm movements. In contrast, it is difficult to reconcile observed saccade trajectories with bang-bang control, or to explain the biological relevance of such factors as jerk or torque change in previous models of arm trajectories.

Moreover, there is no need for the central nervous system to construct highly derived signals to estimate the cost to the movement, which is now variance of the final position or the consequences of this inaccuracy, such as the time spent in making corrective movements[19,20]. Such costs are directly available to the nervous system and the optimal trajectory could be learnt from the experience of repeated movements. Finally, it can be seen that optimal trajectories are inherently smooth. Abrupt changes in the trajectory of the eye or arm require large driving signals which would carry more noise and therefore be suboptimal.

The minimum-variance theory provides a simple, unifying and powerful principle that can be applied to goal-directed movements and implies that signal-dependent noise plays a fundamental role in motor planning. □

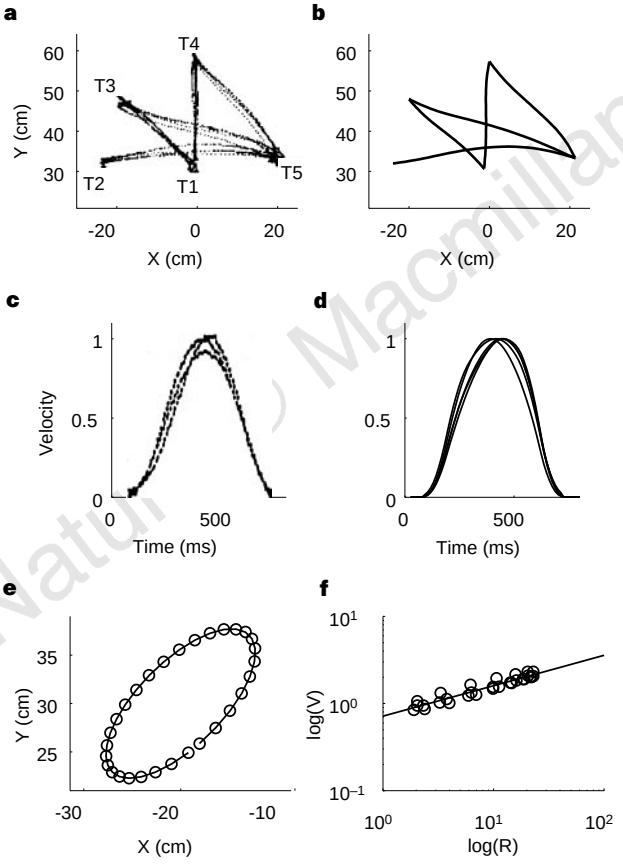

Figure 5 Comparison of empirical and predicted trajectories for a two-joint arm. **a**, Observed hand paths for a set of point-to-point movements (from ref. 15, with permission), and **b**, theoretical optimal hand paths for the same set of movements. The coordinates are centred on the shoulder joint and X and Y directions represent the transverse and sagittal axes respectively. **c**, Observed velocity profiles from T1 to T3 movement in **a**. Note all other movements in **a** showed similar velocity profiles. **d**, Velocity profiles of all the optimal movements shown in **b**, normalized to have a maximum velocity of 1. **e**, Optimal trajectory for drawing an ellipse, the points are equally spaced in time. Note the slowing down at points of high curvature. **f**, Plot of log tangential velocity (V) against log radius of curvature (R). The two-thirds power law predicts $\log(V) = \log(K) + (1-\beta)\log(R)$. Linear regression gives a slope of 0.32 ($r^2 = 0.85$) and hence the value of $\beta = 0.68$.

Methods

We found the optimal trajectories numerically for both linear models of the eye and arm, and a nonlinear model of a two-joint arm, in the presence of signal-dependent white noise in the control signal. The cost function that was minimized was the positional variance across repeated movements summed over the post-movement period.

Linear models. For the linear models of the eye and arm, we consider a single-input single-output discrete-time system under control with a state-update equation given by $\mathbf{x}_{t+1} = A\mathbf{x}_t + \boldsymbol{B}(u_t + w_t)$, where $\mathbf{x}_t$ is the n-dimensional state at time t, u_t is the neural driving signal at t (note that for arm movements, u_t is the neural command signal that activates muscles and is not torque). A is a fixed $n \times n$ matrix and $\boldsymbol{B}$ is a $n \times 1$ vector describing the dynamics of the system; w_t represents white noise on the driving signal, with zero mean and variance ku_t^2, which increases with the magnitude of the control signal, u_t, and represents the signal-dependent noise. By iterating the state-update equation, the distribution of the state at time t can be shown to have a mean

$$\mathrm{E}[\mathbf{x}_t] = A^t\mathbf{x}_0 + \sum_{i=0}^{t-1} A^{t-1-i}\boldsymbol{B}u_i$$

with covariance

$$\mathrm{Cov}[\mathbf{x}_t] = k\sum_{i=0}^{t-1}(A^{t-1-i}\boldsymbol{B})(A^{t-1-i}\boldsymbol{B})^{\mathrm{T}}u_i^2 \qquad (1)$$

The variance of the position at time t, V_t, is given by the appropriate element of the diagonal of $\mathrm{Cov}[\mathbf{x}_t]$. We wish to find the driving signal, $\mathbf{u} = [u_0, u_1, u_2, \ldots, u_{T+R}]^{\mathrm{T}}$, that reaches the desired position at time step T (the movement time) and maintains it for R steps (the post-movement time) and which minimizes the summed positional variance during this post-movement period, $\Sigma_{i=T+1}^{T+R} V_t$ (the cost). This can be formulated as a quadratic programming problem which was solved using Matlab.

For the second-order linear model of the eye, the time constants were 224 and 13 ms (ref. 21). Movement durations were taken from ref. 4. Simulations were performed with a time step of 1 ms and a post-movement fixation period of 50 ms. For the third-order model of the eye, an additional time constant of 10 ms was included. There were negligible changes in the optimal trajectories for post-movement times $R > 20$ ms.

For the one-dimensional arm model, we used the combination of a second-order linear model of muscle and a second-order linear model of the arm's skeletal system which included inertia and viscosity. The time constants of the muscle were taken as 40 and 30 ms and the inertia of the arm was 0.25 kg m^2 and the viscosity was 0.2 N ms rad^{-1} (ref. 23). Simulations were performed with a time step of 10 ms and a post-movement period of 500 ms. There were negligible changes in the optimal trajectories for post-movement times $R > 200$ ms.

To simulate Fitt's law, we assumed that subjects are required to place any part of their finger of width w (taken as 6 mm) within the target of width W with a fixed probability (the success rate). The required accuracy of the movement,

specified as the desired final positional standard deviation, was taken as $(W + w)/r$, where r was taken as 1.96 to achieve a 95% success rate. The movement duration was calculated as the shortest possible time that could achieve this accuracy constraint, given that the signal-dependent noise on the entire motor-neuronal pool had a 1% coefficient of variation.

Nonlinear model. For the nonlinear two-jointed planar arm, we used two linear second-order muscles, as described above, acting on the shoulder and elbow joint of a two-link arm moving in the horizontal plane (arm parameters from ref. 29). The trajectories were parametrized as cubic splines with the knots evenly spaced in time. For the point-to-point movements, 7 cartesian (x,y) knots were used with the first and last points fixed at the start and target locations with zero velocity. 500 movements (650-ms duration, sampled at 10 ms) were simulated with signal-dependent noise to determine the trajectory that minimizes the post-movement variance. The optimal trajectory was found using the simplex algorithm to adjust the knot locations.

For ellipse-drawing movements (duration 600 ms, sampled at 20 ms), the knots represented the proportion of the distance travelled around the ellipse as a function of time. Seven knots were used with the first knot at zero and the last at one. This spline determined the velocity profile of the movement which was confined to an elliptic path. The simplex algorithm was used to find the optimal trajectory.

Received 25 March; accepted 8 June 1998.

1. Bernstein, N. *The Coordination and Regulation of Movements* (Pergamon, London, 1967).
2. Wolpert, D. M. Computational approaches to motor control. *Trends Cogn. Sci.* **1,** 209–216 (1997).
3. Morasso, P. Spatial control of arm movements. *Exp. Brain Res.* **42,** 223–227 (1981).
4. Collewijn, H., Erkelens, C. J. & Steinman, R. M. Binocular coordination of human horizontal saccadic eye-movements. *J. Physiol.* **404,** 157–182 (1988).
5. Fitts, P. M. The information capacity of the human motor system in controlling the amplitude of movements. *J. Exp. Psychol.* **47,** 381–391 (1954).
6. Shadmehr, R. & Mussa-Ivaldi, F. Adaptive representation of dynamics during learning of a motor task. *J. Neurosci.* **14:5,** 3208–3224 (1994).
7. Brashers-Krug, T., Shadmehr, R. & Bizzi, E. Consolidation in human motor memory. *Nature* **382,** 252–255 (1996).
8. Lacquaniti, F., Terzuolo, C. A. & Viviani, P. The law relating kinematic and figural aspects of drawing movements. *Acta Psychologica* **54,** 115–130 (1983).
9. Viviani, P. & Schneider, R. A developmental study of the relationship between geometry and kinematics in drawing movements. *J. Exp. Psychol. HPP* **17,** 198–218 (1991).
10. Enderle, J. D. & Wolfe, J. W. Time-optimal control of saccadic eye-movements. *IEEE Trans. Biomed. Eng.* **34,** 43–55 (1987).
11. Harris, C. M., Wallman, J. & Scudder, C. A. Fourier analysis of saccades in monkeys and humans. *J. Neurophysiol.* **63:4,** 877–886 (1990).
12. Harris, C. M. On the optimal control of behaviour: A stochastic perspective. *J. Neurosci. Meth.* **83,** 73–88 (1998).
13. Hogan, N. An organizing principle for a class of voluntary movements. *J. Neurosci.* **4,** 2745–2754 (1984).
14. Flash, T. & Hogan, N. The co-ordination of arm movements: An experimentally confirmed mathematical model. *J. Neurosci.* **5,** 1688–1703 (1985).
15. Uno, Y., Kawato, M. & Suzuki, R. Formation and control of optimal trajectories in human multijoint arm movements: Minimum torque-change model. *Biol. Cybern.* **61,** 89–101 (1989).
16. Wolpert, D. M., Ghahramani, Z. & Jordan, M. I. An internal model for sensorimotor integration. *Science* **269,** 1880–1882 (1995).
17. Clammam, P. H. Statistical analysis of motor unit firing patterns in human skeletal muscle. *Biophysics J.* **9,** 1233–1251 (1969).
18. Matthews, P. B. C. Relationship of firing intervals of human motor units to the trajectory of post-spike after-hyperpolarization and synaptic noise. *J. Physiol.* **492,** 597–628 (1996).
19. Meyer, D. E., Abrams, R. A., Kornblum, S., Wright, C. E. & Smith, J. E. K. Optimality in human motor performance: Ideal control of rapid aimed movements. *Psychol. Rev.* **98,** 340–370 (1988).
20. Harris, C. M. Does saccadic under-shoot minimize saccadic flight-time? A Monte Carlo study. *Vision Res.* **35,** 691–701 (1995).
21. Robinson, D. A., Gordon, J. L. & Gordon, S. E. A model of the smooth pursuit eye movement system. *Biol. Cybern.* **55,** 43–57 (1986).
22. van Gisbergen, J. A. M., Robinson, D. A. & Gielen, C. C. A. M. A quantitative analysis of generation of saccadic eye movements by burst neurons. *J. Neurophysiol.* **45,** 417–442 (1981).
23. van der Helm, F. C. T. & Rozendaal, L. A. in *Biomechanics and Neural Control of Movement* (eds Winters, J. M. & Crago, P. E.) (Springer, New York, in the press).
24. Kelso, J. A. S., Southard, D. L. & Goodman, D. On the nature of human interlimb coordination. *Science* **203,** 1029–1031 (1979).
25. Lackner, J. R. & DiZio, P. Rapid adaptation to Coriolis force perturbations of arm trajectory. *J. Neurophysiol.* **72,** 299–313 (1994).
26. Sainburg, R. L. & Ghez, C. Limitations in the learning and generalization of multi-joint dynamics. *Soc. Neurosci. Abstr.* **21,** 686 (1995).
27. Flash, T. & Gurevich, I. in *Self-Organization, Computational Maps and Motor Control* (eds Morasso, P. G. & Sanguinetti, V.) 423–481 (Elsevier, Amsterdam, 1997).
28. Goodbody, S. J. & Wolpert, D. M. Temporal and amplitude generalization in motor learning. *J. Neurophysiol.* **79,** 1825–1838 (1998).
29. Kawato, M. in *Attention and Performance, XVI* (eds Inui, T. & McClelland, J.) 335–367 (MIT Press, Cambridge, MA, 1996).
30. Jeannerod, M. *The Neural and Behavioural Organization of Goal-directed Movements* (OUP Psychology Ser. No. 5, Oxford, 1988).

Acknowledgements. We thank S. Goodbody, Z. Ghahramani and M. Pembrey for comments on the manuscript. This project was supported by the MRC, the Wellcome Trust, Help a Child to See charity, the IRIS fund, the Child Health Research Appeal Trust and the Royal Society.

Correspondence and requests for materials should be addressed to C.M.H.

Cortical feedback improves discrimination between figure and background by V1, V2 and V3 neurons

J. M. Hupé, A. C. James*, B. R. Payne*, S. G. Lomber*, P. Girard & J. Bullier

Cerveau et Vision INSERM 371, 18 avenue du Doyen Lépine, 69675 Bron Cédex, France

A single visual stimulus activates neurons in many different cortical areas. A major challenge in cortical physiology is to understand how the neural activity in these numerous active zones leads to a unified percept of the visual scene. The anatomical basis for these interactions is the dense network of connections that link the visual areas. Within this network, feedforward connections transmit signals from lower-order areas such as V1 or V2 to higher-order areas. In addition, there is a dense web of feedback connections which, despite their anatomical prominence[1–4], remain functionally mysterious[5–8]. Here we show, using reversible inactivation of a higher-order area (monkey area V5/MT), that feedback connections serve to amplify and focus activity of neurons in lower-order areas, and that they are important in the differentiation of figure from ground, particularly in the case of stimuli of low visibility. More specifically, we show that feedback connections facilitate responses to objects moving within the classical receptive field; enhance suppression evoked by background stimuli in the surrounding region; and have the strongest effects for stimuli of low salience.

We recorded single units and multiunits (114 single units and 54 multiunits) in areas V1, V2 and V3 of anaesthetized and paralysed macaque monkeys. To study the role of feedback connections from area V5, a small region of the superior temporal sulcus (STS) containing this area was reversibly inactivated by cooling; we then compared the neuronal responses before, during and after STS inactivation. We used visual stimuli consisting of an optimally orientated bar moved across the centre of the receptive field on a background of irregularly distributed, half light and half dark, but lower luminance, square checks (Fig. 1d). In a sequence of interleaved stimulus conditions, the bar and background moved one at a time, or together, in the preferred direction for the cell or its opposite.

Figure 1a–c illustrates a spectrum of effects of the V5 inactivation for single neurons recorded in areas V1, V2 and V3, and stimulated by a bright bar moving in front of a stationary background of lower luminance contrast. A substantial and highly significant decrease in the response to the moving bar is observed in each case during V5 inactivation. Figure 1e, f gives the population data. It is clear that diminution of responses is by far the most frequent effect of V5 inactivation, as observed before for other feedback connections[6,8]. Of the total sample of sites tested, 33% showed a significant decrease ($P < 0.01$) and 6.5% an increase. Similar effects were observed in infragranular and supragranular layers. No effect was observed in layer 4C of area V1.

The role of feedback connections in figure–ground discrimination was suggested to us when we found that the strength of the effect of V5 inactivation depended on the visibility of the stimuli used for testing neurons in area V3, an area that receives a particularly large feedback input from MT/V5 (ref. 9). We com-

* Present addresses: Mammalian Neurobiology and Reproduction, RSBS ANU, GPO Box 475, Canberra, ACT 2601, Australia (A.C.J.); Laboratory of Visual Perception and Cognition, Center for Advanced Biomedical Research, Boston University School of Medicine, 700 Albany Street, Massachusetts 02118, USA (B.R.P. and S.G.L.).